High-Performance Field Effect Transistors Using Electronic Inks of 2D Molybdenum Oxide Nanoflakes

Manal M. Y. A. Alsaif, Adam F. Chrimes, Torben Daeneke, Sivacarendran Balendhran, Darin O. Bellisario, Youngwoo Son, Matthew R. Field, Wei Zhang, Hussein Nili, Emily P. Nguyen, Kay Latham, Joel van Embden, Michael S. Strano, Jian Zhen Ou,* and Kourosh Kalantar-zadeh**

Planar 2D materials are possibly the ideal channel candidates for future field effect transistors (FETs), due to their unique electronic properties. However, the performance of FETs based on 2D materials is yet to exceed those of conventional silicon based devices. Here, a 2D channel thin film made from liquid phase exfoliated molybdenum oxide nanoflake inks with highly controllable substoichiometric levels is presented. The ability to induce oxygen vacancies by solar light irradiation in an aqueous environment allows the tuning of electronic properties in 2D substoichiometric molybdenum oxides (MoO_{3-x}). The highest mobility is found to be ≈600 $cm^2 V^{-1} s^{-1}$ with an estimated free electron concentration of ≈1.6×10^{21} cm^{-3} and an optimal I_{On}/I_{Off} ratio of >10^5 for the FETs made of 2D flakes irradiated for 30 min ($x = 0.042$). These values are significant and represent a real opportunity to realize the next generation of tunable electronic devices using electronic inks.

1. Introduction

The emergence of 2D semiconductors, which are made of single or few layers of crystal unit cell thickness components, has led to a range of unique chemical and physical properties that don't exist in their bulk counterparts.[1–4] In particular, the quantum well effect together with in-plane free charge transport are features that make the 2D semiconductors attractive as channel materials for field effect transistors (FETs).[2–5]

Semiconducting members of the transition metal dichalcogenide (TMD) family is now form a widely studied category of 2D materials. For developing FETs, a typical representative is 2D molybdenum disulfide (MoS_2) with reported mobilities in the range of 10–1000 $cm^2 V^{-1} s^{-1}$ and as exfoliated carrier concentration of ≈10^{19} cm^{-3} in a single layer.[3,6–8] Other few-layered TMDs such as molybdenum diselenide ($MoSe_2$; ≈10^{19} cm^{-3}), tungsten disulfide (WS_2; ≈10^{16} cm^{-3}), and tungsten diselenide (WSe_2; ≈10^{18} cm^{-3}) have charge mobilities that likewise reach a few hundred $cm^2 V^{-1} s^{-1}$. [6,9–11] These numbers are still not competitive with reference to those of conventional silicon based devices.[5,12] There are a few issues that currently affect the potentials of FETs based on TMDs. In order to develop high transconductance FETs in general, the drain and source electrode contacts should show the smallest barrier for the exchange of free carriers,[13] and the free carrier concentration should be increased. Doping TMDs is known to produce enhanced carrier concentration of 6×10^{18}, 2.5×10^{19}, and 10^{20} cm^{-3} for few-layer WS_2, WSe_2, and MoS_2, respectively.[13–15] Such concentration can make the electrode contacts more ohmic. However, their mobility still remains subdued. The free carrier mobilities in TMDs are limited by the Coulomb scattering effect given TMDs small relative dielectric constants (κ).[16] The mobility is even more degraded in highly doped TMDs.[13–15]

Semiconducting 2D transition metal oxides (TMOs) have attracted less attention compared to 2D TMDs due to their generally wider bandgap energies and low carrier concentrations in their stoichiometric states.[17] However, selected TMOs have some remarkable properties that can benefit FETs such as a large κ, which reduces the Coulomb scattering effect, while providing

M. M. Y. A. Alsaif, Dr. A. F. Chrimes, Dr. T. Daeneke, W. Zhang, E. P. Nguyen, Dr. J. Z. Ou, Prof. K. Kalantar-zadeh
School of Electrical and Computer Engineering
RMIT University
Melbourne, Victoria 3001, Australia
E-mail: s3372431@student.rmit.edu.au; jianzhen.ou@rmit.edu.au; kourosh.kalantar@rmit.edu.au

Dr. S. Balendhran, Dr. H. Nili
Functional Materials and Microsystems Research Group
RMIT University
Melbourne, Victoria 3001, Australia

D. O. Bellisario, Y. Son, Prof. M. S. Strano
Department of Chemical Engineering
Massachusetts Institute of Technology
Cambridge, MA 02139, USA

Dr. M. R. Field
RMIT Microscopy and Microanalysis Facility
RMIT University
Melbourne, Victoria 3001, Australia

Prof. K. Latham, Dr. J. van Embden
School of Applied Sciences
RMIT University
Melbourne, Victoria 3001, Australia

Dr. J. van Embden
CSIRO Manufacturing Flagship
Bayview Avenue
Clayton, Victoria 3168, Australia

DOI: 10.1002/adfm.201503698

the possibility to accommodate ionic dopants to manipulate the material's electronic properties.[16,17] Molybdenum trioxide (MoO_3), a member of the TMO family, is a chemically stable *n*-type semiconductor with a high dielectric constant.[16–19] It is well known that the α-MoO_3 crystal phase has a layered structure. Furthermore, its electronic bandgap can be manipulated by ionic intercalation processes (commonly hydrogen and alkali metal ions). In particular, hydrogen ion (H^+) intercalation has been well studied in α-MoO_3 and allows to tune the material's physicochemical properties, leading to intercalated MoO_3 compounds and eventually substoichiometric molybdenum oxides (MoO_{3-x}).[17] The family of MoO_{3-x} normally includes molybdenum oxides with substoichiometric levels (x) in the range of $0 < x < 1$. Most compounds of MoO_{3-x} ($0 < x \leq 0.125$) such as Mo_9O_{26} and Mo_8O_{23} show semiconducting behavior, while other phases with higher x ($0.125 \leq x < 1$), such as Mo_4O_{11}, are quasimetallic.[20–25] When $x = 1$, it forms a thermodynamically stable semiconducting compound (MoO_2) of reduced bandgap.[26–28] Single substoichiometric oxide flakes have been incorporated in 2D FETs.[16] Despite the fact that reduced molybdenum oxides demonstrate mobilities exceeding 1000 $cm^2\ V^{-1}\ s^{-1}$ their I_{On}/I_{Off} ratios are poor as there is still no report on the optimum oxygen vacancies required to obtain the most efficient FET operation.[16]

In addition to developing FETs using single 2D flakes, establishing high-performance FETs using thin films based on 2D flake stacks is an important challenge.[29] Such films are generally made using so called "electronic ink," which in our case are suspensions of 2D flakes, that can be deposited onto substrates using a variety of techniques, including printing, drop-casting, and templating.[29–31] Such films can be used in flexible electronics, touch screens, sensors, RFID tags, photovoltaic cells, and electronic textiles.[2,32,33] Some of the best reports on thin film based FETs that incorporate graphene flakes only reach mobilities near 100 $cm^2\ V^{-1}\ s^{-1}$ with poor I_{On}/I_{Off} ratios.[32] There are also recent reports on incorporating thin films of 2D WS_2 flakes.[33] However, although the reported mobilities are high, the I_{On}/I_{Off} ratios were too low for establishing FETs.

Here we produce electronic inks of 2D MoO_{3-x} flakes and use them for developing channels for FETs with extraordinary abilities. We use a solar light irradiation based method to control the oxygen vacancies and free electron concentration (N) in liquid-phase exfoliated (LPE) 2D MoO_{3-x} flakes. Through the controlled manipulation of x, we show that the carrier concentration, energy band edge, and carrier charge mobility in 2D MoO_{3-x} based FETs can be tuned. Furthermore, these parameters are evaluated as a function of the 2D flakes' stoichiometry. Finally, we present tunable FETs based on 2D MoO_{3-x} nanoflakes with different substoichiometric levels and demonstrate that the optimal substoichiometric value using LPE technique with the maximum transconductance is obtained.

2. Results and Discussion

2.1. Characterization of 2D Molybdenum Oxide Flakes

Suspensions of 2D molybdenum oxide flakes were prepared in a 50:50 (v/v) ethanol:water mixture to form the electronic inks, as described in the Experimental Section. Samples of equal volume and concentration were irradiated by a solar simulator for 5 min, 10 min, 20 min, 30 min, 1 h, 2 h, and 5 h to obtain the substoichiometric 2D MoO_{3-x} flake suspensions.

Figure 1a shows the schematic crystal structure of pristine α-MoO_3, wherein each molybdenum atom bonds to edge-sharing, corner-sharing, and unshared terminal oxygen atoms.[34] The ionization energy (IE) of the pristine (initial) sample of MoO_3 was measured by photoelectron spectroscopy in air (PESA), which correlates to the valence band maximum (VBM) and was found to be −5.58 eV with respect to vacuum (vac),[35] which is below the water oxidation potential ($H_2O/O_2 \approx -5.3$ eV respect to vac) in our solar light induced reaction conditions (see Note 1 and Figure S1 in the Supporting Information). As such, the photoexcited electrons remain in the conduction band (CB) and H^+ ions are intercalated into 2D α-MoO_3.[28,36] The electrons in the CB are strong reductants, providing the driving force for the intercalation reaction within the MoO_3 structure (conduction band minimum (CBM) = −2.73 eV with respect to vac).[28,35,36] The intercalated H^+ ions are mostly bonded to edge-shared oxygen and terminal oxygen atoms, which forms OH_2 groups; hence transforming 2D MoO_3 into 2D H_xMoO_3 (Figure 1b).[28,34] This causes the increase of interlayer spacing.[37] However, the OH_2 groups are not stable in the presence of environmental perturbations (e.g., heat) and are eventually released from their original positions in the crystal lattice, leaving alone oxygen vacancies and subsequently forming substoichiometric 2D MoO_{3-x} (Figure 1b).[34] This rapid process of defect formation also causes crystal deformation and cracking in both intralayer and interlayer directions, hence reducing the lateral dimensions and thickness of the flakes.[37] The average lateral dimensions of molybdenum oxide flakes before and after solar light illumination for different durations were investigated using dynamic light scattering (DLS) (Figure 1c; Figure S2, Supporting Information). The average lateral dimension of the initial MoO_3 flakes is ≈170 nm, while after 5 min irradiation it is reduced by approximately 10%. Interestingly at 30 min irradiation duration, the average lateral dimension of flakes falls to ≈130 nm. The dynamics of the lateral dimension reduction changes after 30 min of irradiation and the average value reaches ≈80 nm at the 5 h mark. Transmission electron microscopy (TEM) verifies that the lateral dimensions of 2D flakes after 5 h irradiation are distinctly reduced (Figure 1d,e; Figure S3, Supporting Information). The thicknesses of the nanoflakes before and after 5 h irradiation were also assessed using atomic force microscopy (AFM). Figure 1f,g shows that the 2D morphologies of the flakes are retained regardless of the light irradiation duration. The initial average flake thickness is made of around five layers, while they are reduced to an average of three layers after the 5 h irradiation process (Figure S4, Supporting Information). As such, exfoliation continues during the whole solar irradiation process. The effect of different solvent compositions on the lateral dimensions of the initial 2D MoO_3 flakes is also investigated by using the DLS technique (see the Experimental Section and Figure S5 in the Supporting Information). We find that the suspension composition of 50:50 (v/v) ethanol:water mixture produces the largest lateral dimension of the flakes. As such, this suspension composition is used for producing the electronic ink in order to assure that the least charge carrier

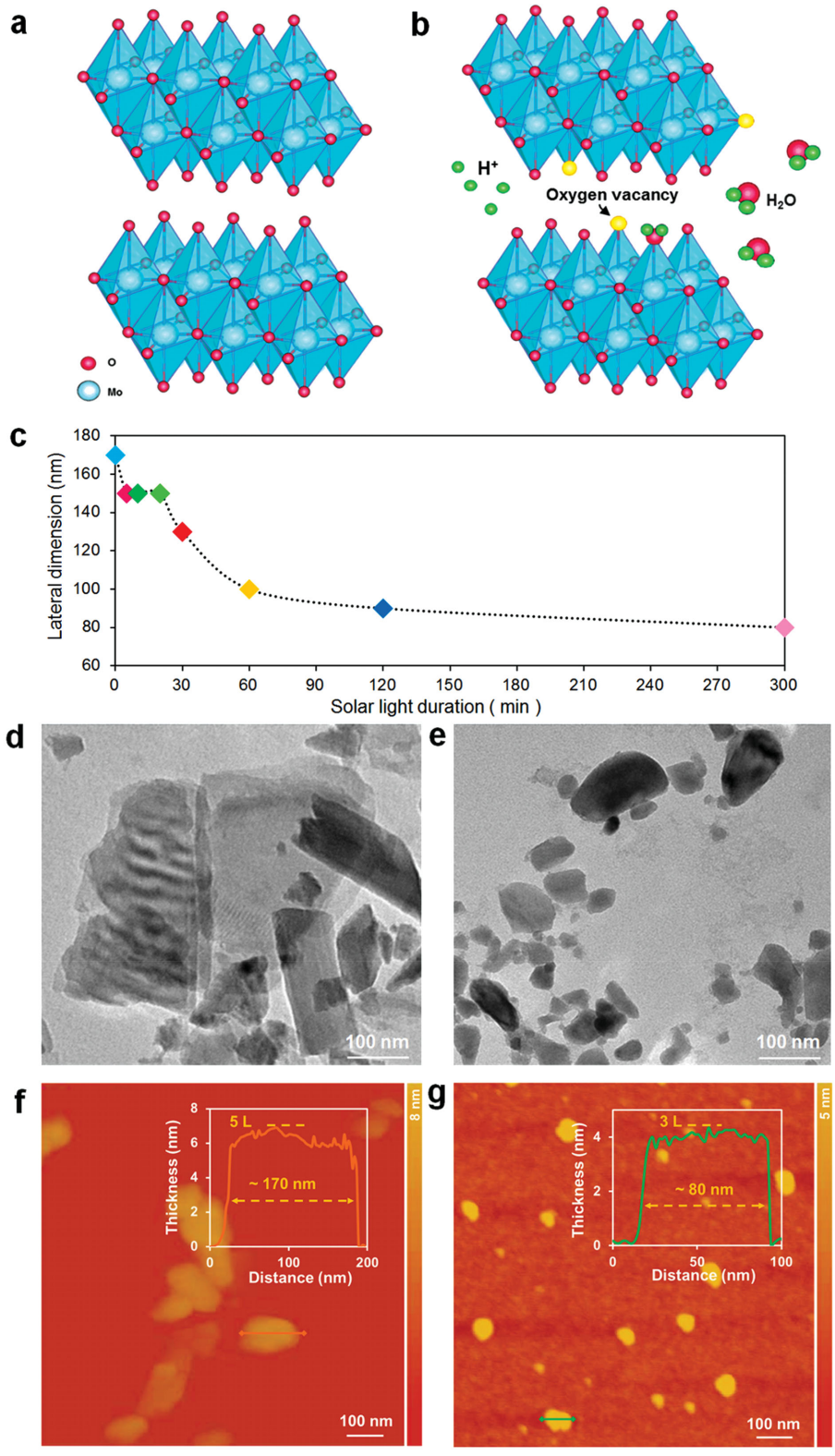

Figure 1. Morphological characterizations of 2D molybdenum oxide flakes. a) The schematic of α-MoO_3. b) The schematic of hydrogen ions intercalation of 2D α-MoO_3 after solar irradiation. c) The lateral dimensions of the molybdenum oxide flakes after different durations of simulated solar light irradiation. d) A TEM image of the initial 2D α-MoO_3 nanoflakes. e) A TEM image of 2D nanoflakes after 5 h of solar light irradiation. f) The AFM image of the initial 2D MoO_3 nanoflakes with the average thickness of ≈5 layers. g) The AFM image of 2D nanoflakes after 5 h of solar light irradiation with the average thickness of ≈3 layers.

scattering is generated by the boundaries during the transfer of a charge from one flake to another. Moreover, the concentration of the 2D MoO_3 flakes in the suspension is measured to be ≈0.018 mg mL^{-1} (details are presented in Note 2 and Figure S6 in the Supporting Information).

The initial 2D molybdenum oxide nanoflakes are made of crystalline orthorhombic α-MoO_3 according to the X-ray diffraction (XRD) pattern (Figure S7, Supporting Information). **Figure 2**a shows a high-resolution TEM (HRTEM) image highlighting the lattice fringes of the 2D nanoflakes. A spacing of 0.39 nm is observed associated with the (1 0 0) plane of α-MoO_3. The corresponding selected area electron diffraction (SAED) pattern (Figure 2b) clearly distinguishes diffraction spots representing the (2 0 0) and (0 0 2) planes of α-MoO_3.[28,38] However, after 5 h solar light exposure, some of the lattice fringes appear disordered as a consequence of H^+ intercalation (Figure 2c). This disorder is confirmed from the polycrystalline ring SAED pattern (Figure 2d). The intercalation of the H^+ ions into the crystal lattice eventually produces cracks and splits the crystal into smaller sizes.[39]

To investigate the evolution of this intercalation process, Raman spectra of 2D molybdenum oxide for different solar illumination durations were obtained (**Figure 3**a). Strong Raman peaks are observed for the initial sample which are associated to α-MoO_3 (see Note 3 in the Supporting Information for further discussion).[28,34] New peaks appear after 30 min of solar light exposure, which can be assigned to MoO_{3-x}, suggesting the appearance of oxygen vacancies.[40,41] X-ray photoelectron spectroscopy (XPS) was used for identifying the substoichiometry of the 2D flakes (Figure 3b). The doublets at 235.98 and 232.68 eV are attributed to the binding energies of the $3d_{3/2}$ and the $3d_{5/2}$ orbital electrons of Mo^{6+}, respectively.[19,28] The integrated areas of the two doublets are in a 2:3 ratio and the energy split between them is 3.1 eV, in agreement with α-MoO_3.[17] Two peaks centered at 234.58 and 231.28 eV appear in the Mo 3d core level spectrum after 5 min of solar light irradiation. These peaks are at lower binding energies compared to Mo^{6+}, indicating the appearance of the Mo^{5+} oxidation state within the flakes. The intensities of these Mo^{5+} peaks, which are correlated with the substoichiometry of molybdenum oxide flakes, increase with the irradiation duration.[28] The substoichiometric level in 2D molybdenum oxide flakes prepared here is lower than reported in our previous work in which an acetonitrile solvent was used.[28] This may be due to the fact that acetonitrile has a higher dispersion solubility parameter (δ_d = 64.3 and a surface tension of 27.6 mN m^{-1}) than ethanol (δ_d = 60.4 and surface tension of 22 mN m^{-1}),[42] facilitating the exfoliation process and producing surface areas for the intercalation process.[43]

During the formation of an oxygen vacancy in the crystal structure upon light exposure, the Mo^{6+} neighboring the oxygen vacancy in the MoO_3 lattice is reduced to Mo^{5+}, injecting an electron to the CB.[16,34] This injected electron is delocalized within the layers and acts as a Drude-model-like free electron,[16] hence modulating the electronic band structure of the 2D flakes.[16] The N for different light irradiation durations is estimated from the Mo^{5+}/Mo^{6+} area ratio in MoO_{3-x}, which extracted from the XPS measurements (**Table 1**a; Figure S8, Supporting Information). It is found that N and oxygen vacancies both increase with the solar light duration. This increase in N shifts the Fermi energy level (E_F) upward toward the CB (Figure 3c; Table S1, Supporting Information).[44] It is important to note that by introducing oxygen vacancies a new occupied state appears within the E_g of MoO_{3-x}, labeled d in Figure 3d. This defect state arise because an O^{2-} ion is removed from the valence-band spectra of MoO_{3-x}.[45] The previously empty 4d band of MoO_3 becomes

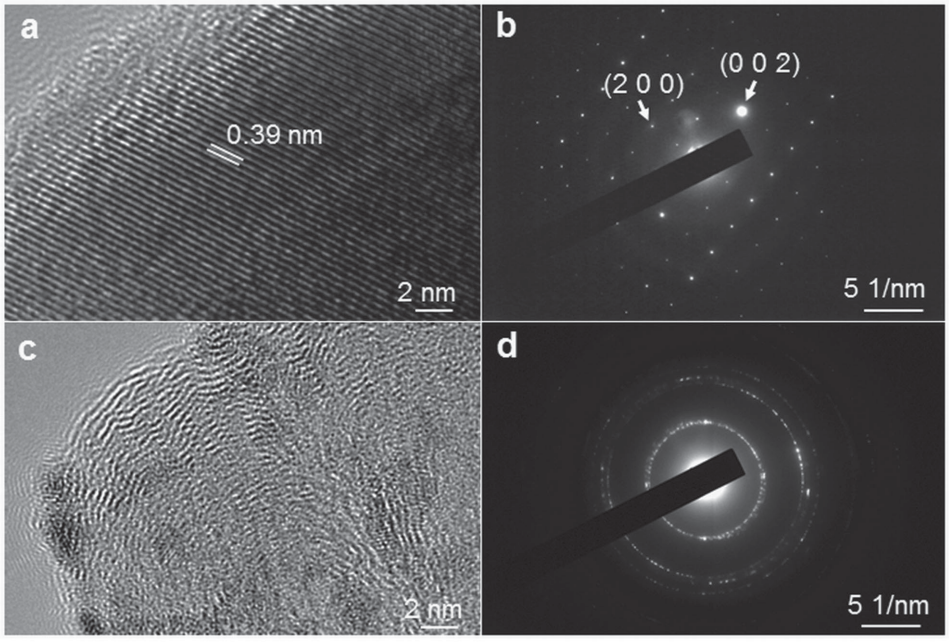

Figure 2. Crystal structures of 2D molybdenum oxide flakes. a) A HRTEM image of the initial 2D α-MoO_3 nanoflake and b) the corresponding SAED pattern. c) A HRTEM image of the 2D nanoflake after 5 h of solar light irradiation and d) its corresponding SAED pattern.

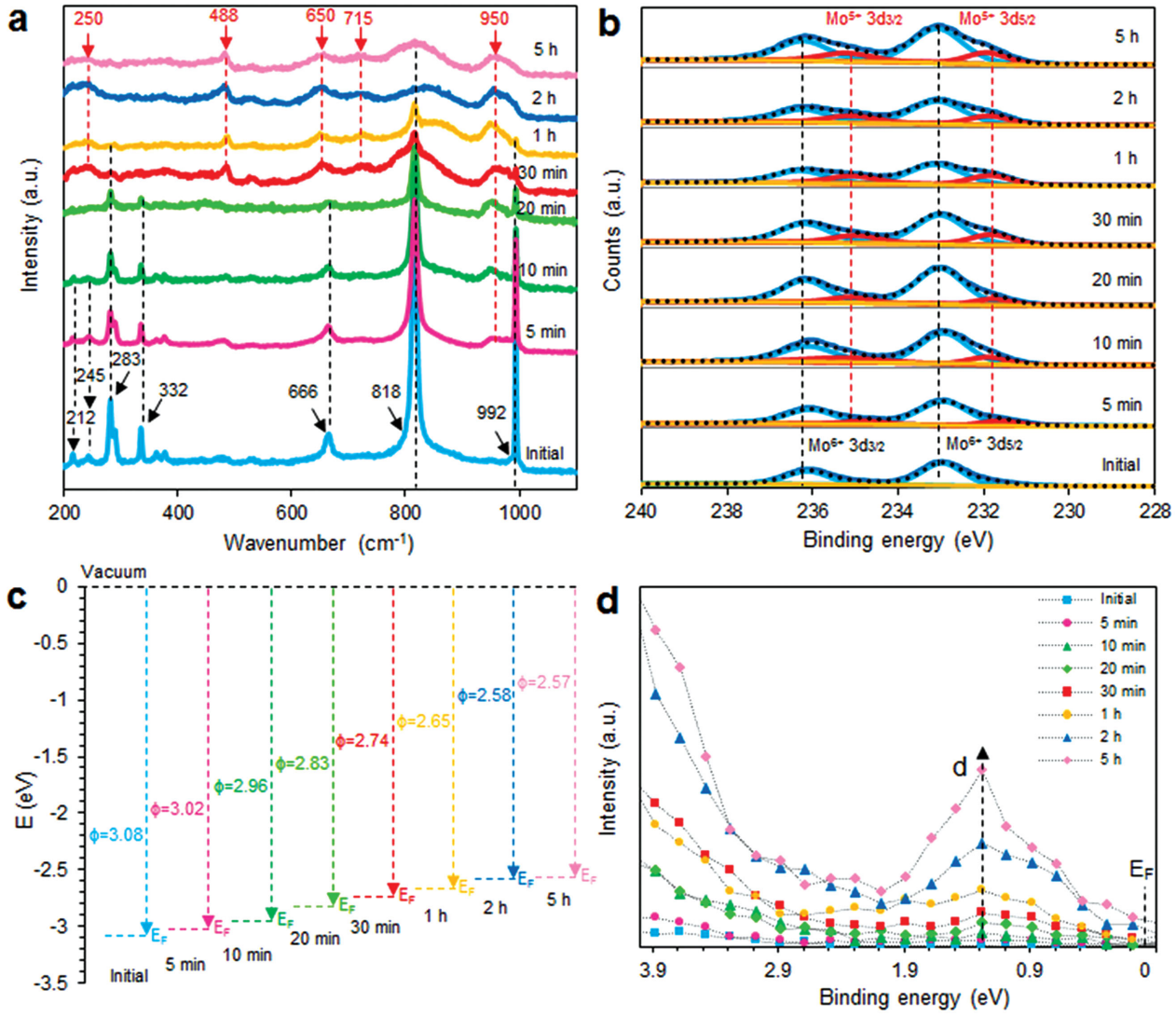

Figure 3. Structural characterizations and electronic band structures of 2D molybdenum oxide flakes obtained at different light exposure durations. a) The Raman spectra of 2D molybdenum oxide flakes upon different solar light durations. b) XPS Mo3d spectra of the 2D flakes at different solar light irradiation durations. c) The energy level diagram with respect to vac showing the E_F of the 2D flakes after different solar irradiation duration. The E_F is evaluated from PESA measurements (Figure S9, Supporting Information) and VBM position by the valence photoemission spectroscopy (Figure S10, Supporting Information). d) The valence photoemission spectra of substoichiometric 2D molybdenum oxides at low binding energy region for different solar irradiation durations.

partially occupied with electrons, giving rise to the defect band seen close to the E_F (1.28 eV below E_F) which is enhanced in the intensity by increasing the solar light duration (Figure 3d).[45]

Prolonging the solar irradiation of the flakes moves their valence band (VB) (Table S1, Supporting Information) closer to that of the work function of gold, which forms the FET drain and source electrodes. Molybdenum oxide is a well-known hole extracting material that can exchange electrons at its VB,[35,46] coinciding gold's E_F that makes a small barrier contact. The enhancement in the electron concentration and tuning of the VB modify the system to obtain the optimal I_{On}/I_{Off} ratio for FETs made of 2D MoO_{3-x} flakes at $x = 0.042$ (30 min irradiation), which will be discussed later. Interestingly, the estimated E_g of MoO_{3-x} for samples of $x = 0.042$ and $x = 0.125$ (5 h irradiation) are 2.74 and 2.82 eV, respectively (Figure S11a,b, Supporting Information). Thus, the CBM for both of these samples were evaluated to be ≈2.60 and 2.56 eV, respectively (Figure S11a,b, Supporting Information). The E_F of both the initial and solar light exposed flakes never exceeds the CBM and thus the highly doped flakes should still remain semiconducting.

2.2. Fabrication and Characterization of FETs Based on 2D Molybdenum Oxide Flakes

Figure 4a–c shows a schematic highlighting the fabrication process of FETs using inks of 2D molybdenum oxide flakes. Details are presented in the Experimental Section. From the

Table 1. Summary of materials and corresponding FETs characteristics: a) estimated free electron concentration for different solar light durations. b) Electrical characteristics of FETs based on 2D molybdenum oxides of different substoichiometric levels (x).

Solar light duration	Mo^{5+}/Mo^{6+} ratio	Substoichiometric (x) of MoO_{3-x}	Estimated free electron concentration [cm^{-3}]
		a)	
Initial (0 min)	0	0	2.24×10^{18} [44]
5 min	0.050	0.025	9.85×10^{20}
10 min	0.063	0.032	1.23×10^{21}
20 min	0.071	0.035	1.41×10^{21}
30 min	0.083	0.042	1.64×10^{21}
1 h	0.125	0.063	2.46×10^{21}
2 h	0.167	0.084	3.28×10^{21}
5 h	0.250	0.125	4.92×10^{21}
		b)	
Device with x	I_{On}/I_{Off} ratio	g_m [μS]	μ_{FE} [$cm^2\ V^{-1}\ s^{-1}$]
0	4.5×10^2	0.083	14.5
0.025	9.4×10^3	0.283	49.4
0.032	3.2×10^4	0.683	119
0.035	3.8×10^4	2.70	471
0.042	3.0×10^5	3.45	600
0.063	3.8×10^3	1.85	323
0.084	1.6×10^2	0.268	46.8
0.125	1.2×10^2	0.143	25.0

examples shown in Figure 4d,e, the drop-casted thin films all have smooth surfaces and are formed by horizontally interconnected 2D molybdenum oxide flakes. Within the FET channels, the 2D nanoflakes are horizontally restacked on the top of each other as evidenced by both cross-sectional scanning electron microscopy (SEM) and scanning probe microscopy (SPM). These data confirm that the FET channels are made of true 2D components.

We characterized the FETs using a semiconductor parameter analyzer and shielded probe station at room temperature. A back gate voltage was applied to the silicon substrate and the two electrodes act as drain and source terminals (Figure 4c). I–V curves of the FETs based on 2D molybdenum oxide flakes of different x are illustrated in Figure S12 in the Supporting Information. The drain-source current (I_{SD}) versus applied gate voltage (V_G) from −10 to 1 V are extracted from Figure S12 in the Supporting Information and presented in **Figure 5**a. For all devices, their I_{SD} are enhanced with the increase of the applied gate voltages. They are typical characteristics of channel FETs and confirm the semiconducting character of the 2D molybdenum oxide flakes regardless of their x values.[16] It is found that I_{SD} enhances when x increases from 0.025 to 0.042. However, for the FET devices made of flakes with $x > 0.063$, the I_{SD} dramatically decrease and eventually drop much below the initial value at $x = 0.125$.

Figure 5b shows the I_{On}/I_{Off} ratio as a function of x. The highest I_{On}/I_{Off} ratio is $\approx 3.0 \times 10^5$ for FETs made of flakes of $x = 0.042$. However, the ratio is significantly reduced to $\approx 1.2 \times 10^2$ at $x = 0.125$ (Table 1b). As previously discussed, a combination of the optimum barrier contact and electron concentration contributes to the optimum I_{On}/I_{Off} ratio of the FETs made of 2D flakes with $x = 0.042$. Considering that an I_{On}/I_{Off} ratios greater than 10^4 are acceptable for establishing functional FETs,[1] here, the obtained ratios for many of the x values are industrially plausible. The introduction of the oxygen vacancies produces a defect state nearly 1.28 eV below the E_F. Given the heavy doping of the materials, they may behave like degenerate semiconductors with the E_F very close to the CBM. In such a case, we may view the system as possessing a small quasibandgap that can be readily turned off at low gate voltages. This can also be another reason that contributes to the large I_{On}/I_{Off} ratio of the optimum semiconducting effect obtained at $x = 0.042$. The transconductance (g_m) of the FETs at $V_{SD} = 100$ mV is extracted and calculated from their I–V characteristics using [47]

$$g_m = dI_{SD}/dV_G \quad (1)$$

The corresponding carrier field effect mobilities (μ_{FE}) are determined using Equation (3) and shown in Table 1b

$$\mu_{FE} = \frac{L}{WC_iV_{SD}} \times g_m \quad (2)$$

where L and W are the channel length and width, respectively. C_i is 1.91×10^{-8} F cm^{-2} which is the capacitance per unit area between the channel and the back gate.[7] The calculated g_m and the measured μ_{FE} are presented in Figure 5c,d and Table 1b. The highest value of g_m and μ_{FE} were ≈3.45 μS and ≈600 $cm^2\ V^{-1}\ s^{-1}$, respectively, for the device of $x = 0.042$ (30 min irradiation), while the device of $x = 0$ (initial sample) had the lowest g_m of ≈0.083 μS and μ_{FE} of ≈14.5 $cm^2\ V^{-1}\ s^{-1}$. Interestingly, the value of μ_{FE} for the FETs of $x = 0.042$ is significantly higher than the mobility of most of thin film transistors based on typical mono- or few-layered TMDs.[3,6,8,9,13,48] The optimal μ_{FE} that occurs for the device at $x = 0.042$ corresponds to $Mo^{5+}/Mo^{6+} = 0.083$, coinciding orthorhombic to monoclinic phase change, which possibly results in gaining optimal semiconducting properties at this substoichiometry. It is worthwhile to define a virtual free carrier mobility per flake by considering the average number of flakes in thickness (from Figure 4 d,e, it is ≈95 layer in a 850 nm thick channel and MoO_3 relative (static) dielectric constant of 35)[16] that is equal to ≈6 $cm^2\ V^{-1}\ s^{-1}$ per flake. This value is still a remarkably large, taking into account that the high electron scattering occurs at the flake boundaries. The effect of the drop casted film thickness on the performance of FETs is also investigated (Note 4 and Figure S13, Supporting Information).

The μ_{FE} of 2D MoO_{3-x} flake based FETs was assessed as a function of N (Details are presented in Note 5 and Figure S14 in the Supporting Information). The assessed μ_{FE} and the theoretical μ_{Total} (Matthiessen's rule) values of carrier mobilites are presented in Figure 5d and Figure S14 in the Supporting Information. The trend of μ_{FE} can be explained by various electron scattering mechanisms. It is found that for $x < 0.042$, the main limiting factor for μ_{FE} is the ionized charged scattering effect (Coulomb scattering).[49] As discussed in the Section 1, MoO_{3-x}

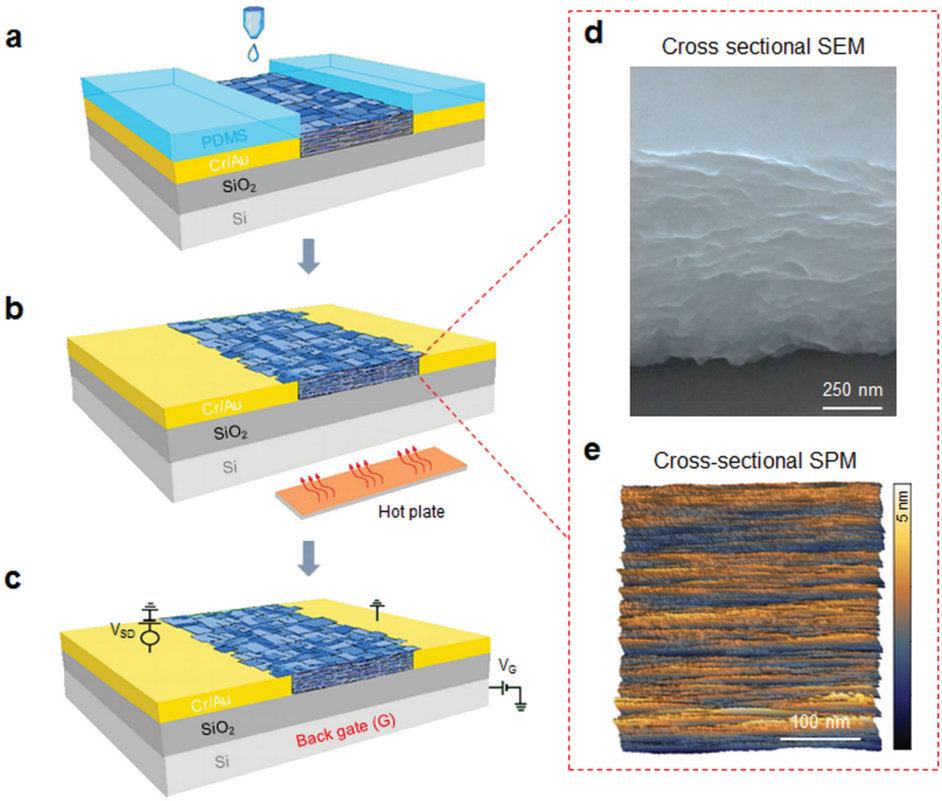

Figure 4. Fabrication of FETs based on 2D molybdenum oxide flakes. a,b) Illustration of the fabrication steps of a FET based on 2D molybdenum oxide flakes. c) The configuration diagram of the electrical connections of a FET. d) Cross-sectional SEM image and e) cross-sectional SPM image revealing that the FET channel is made of orderly restacked 2D molybdenum oxide flakes in a planar manner.

with its large relative (static) dielectric constant screens the Coulomb charges.[16,28] This reduces ionized charge scattering effect and produces remarkable free charge carrier mobility in the FET channels. Subsequently, at $x = 0.042$ and $x = 0.063$ both ionized charge scattering and acoustic deformation potential scattering become the dominant effects. For the 2D flakes with $x > 0.063$, optical phonon scattering becomes the governing effect.[49,50] It should be noted that the charge carrier mobilities of some highly crystalline materials are reported to be larger than their polycrystalline counterparts due to the reduction of structural defect densities when their mobilities are limited by phonon scattering.[51,52] However, in the case of 2D MoO_{3-x}, its mobility is mainly limited by ionized charge scattering when $x < 0.042$ according to the calculation shown in Figure S14 (Supporting Information). The solar light irradiated flakes with lower crystallinity exhibit much more enhanced free electron concentration (N) due to the generation of oxygen vacancies and hence, the mobility is increased compared to that of initial highly crystalline flakes, which is similar to the cases of some other 2D systems.[49,53]

It is important to emphasize that the 2D flakes forming the thin films are restacked horizontally; potentially helping the planar conduction of free charge carries within the FET channels, hence enhancing the mobility. From Figure 5d, we see that the measured μ_{FE} is still almost an order of magnitude smaller than the calculated μ_{Total}, which may be the result of significant grain boundary scattering (μ_{GB}) existing between the interconnected flakes given their relatively small lateral dimensions (≈100–200 nm).[54] Moreover, the decrease in μ_{FE} for $x > 0.063$ is much larger than the calculated trend, implying an increased effect of μ_{GB} as the flake sizes are dramatically reduced to below 100 nm. It is also possible that more defects, which act as charge traps, are formed when 2D MoO_{3-x} flakes become highly substoichiometric.[55]

3. Conclusion

We developed electronic inks based on 2D MoO_{3-x} nanoflakes obtained by a LPE method, for which the substoichiometric and Fermi levels as well as free electron concentration could be manipulated in a highly controllable manner by varying the light irradiation duration. FETs were fabricated using these inks by a drop-casting process, forming films made of layers of horizontally restacked 2D flakes. By investigating the performances of our FETs as a function of x under different solar irradiation time, we found that the device irradiated within 30 min ($x = 0.042$) reached the highest charge carrier mobility of ≈600 $cm^2 V^{-1} s^{-1}$ with an I_{On}/I_{Off} ratio of ≈3.0×10^5. We demonstrated that a gap state appears in the bandgap of MoO_{3-x}, which contributed to the semiconducting behavior of the flakes. The horizontal restacking of the flakes and the confinement of the electric field lines by a high dielectric medium of MoO_{3-x} also contributed to the high free carrier charge mobility.

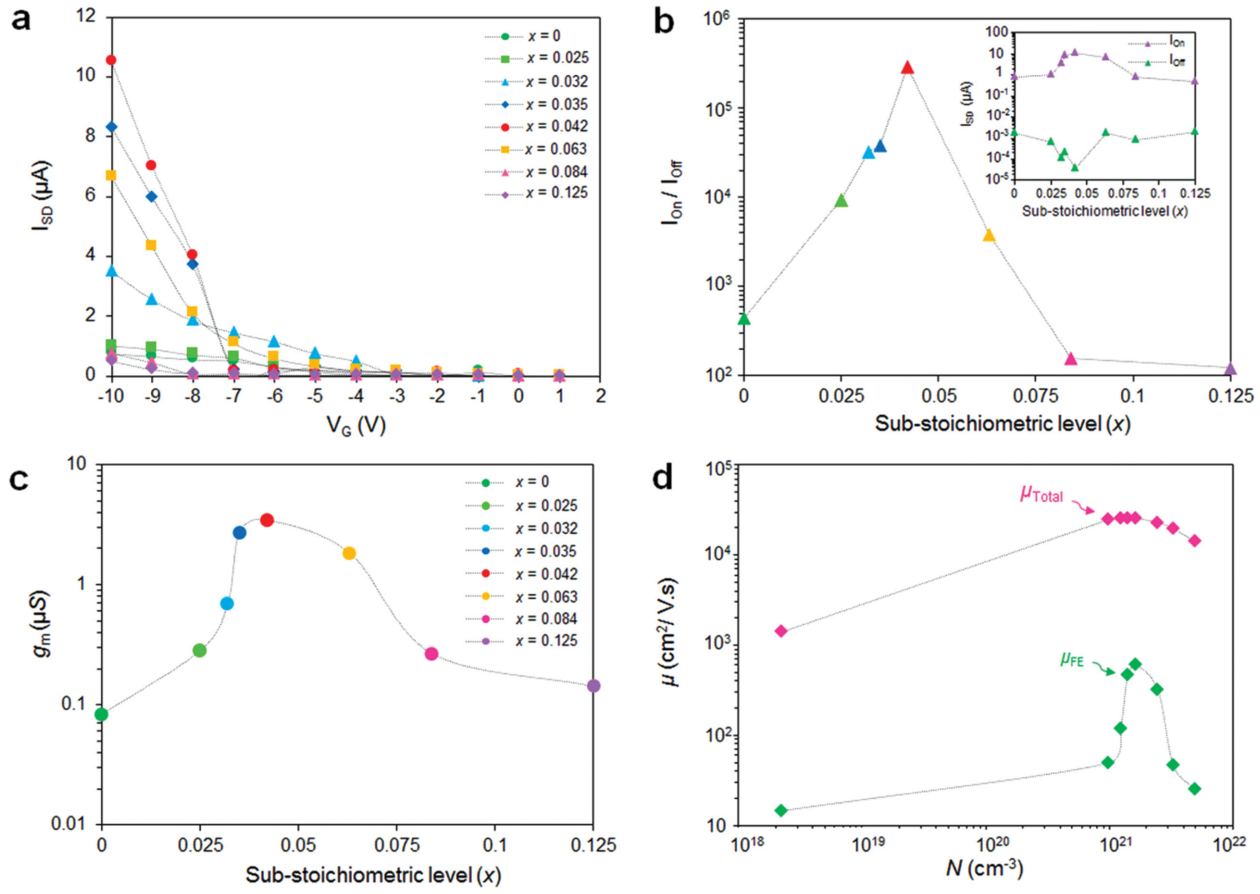

Figure 5. Electrical characteristics of FETs based on films of 2D molybdenum oxide flakes for different substoichiometric levels (x). a) Current versus applied gate bias for the FETs with different x values and b) corresponding I_{On}/I_{Off} ratios for the FETs. The inset is the I_{On} and I_{Off} with respect to x values. c) Corresponding transconductance (g_m) of the FETs and d) the total calculated charge carrier mobility according to Matthiessen's rule and experimental effective mobility as a function of N at room temperature.

Given the scalability and reliability of the LPE technique and the ease of irradiation process for tuning the material, the electronic ink of 2D MoO_{3-x} flakes is promising for future ultra-high-performance printed nanoelectronic and optoelectronic devices.

4. Experimental Section

2D Molybdenum Oxide Flakes Synthesis and FET Device Fabrication: 3 g of MoO_3 powder (99% purity, China Rare Metal Material Co.) was ground with 0.6 mL ethanol for 30 min. The powder was then dispersed in ethanol/water (50:50 (v/v) ethanol:water) mixture (45 mL), subjected to probe-sonication (Ultrasonic Processor GEX500) for 120 min at 125 W, and then centrifuged at 6000 rpm for 30 min at room temperature. To obtain the electronic inks, the supernatant containing high concentration of 2D MoO_3 flakes was collected and transferred into small containers with 3 mL volume each. The supernatant samples were irradiated under the solar simulator (Abet Technologies LS-150) at different time intervals of 5 min, 10 min, 20 min, 30 min, 1 h, 2 h, and 5 h and subsequently drop-casted at the fixed amount of 50 μL on substrates for characterization and FET fabrication. Au/Cr (150/50 nm) electrodes were deposited onto clean n-doped silicon wafer substrates with 500 nm thick SiO_2 surface layers using an electron beam evaporation process and subsequently patterned by conventional photolithography. The spacing between the electrodes was set to 50 μm. A polydimethylsiloxane (PDMS) reservoir was used for the drop-casting process. The drop-casted devices were then annealed at 75 °C to remove the trapped water and organic molecules between the flakes and kept at room temperature for electrical investigations. The thicknesses of all FET channels were equally set to ≈850 nm. The extended Raman spectra of the drop-casted films (Note 6 and Figure S15, Supporting Information) reveal that there was no observable peak appearing beyond 1000 cm^{-1}, which indicates that the organic residue in the films was fully evaporated.

Investigation of Different Solvent Compositions: The grinding process of 3 g of MoO_3 with 0.6 mL of ethanol, for 30 min was repeated four times. The four grounded samples were then dispersed in 45 mL of ethanol (100%), 70:30 (v/v) ethanol:water mixture, 30:70 (v/v) ethanol:water mixture, and water (100%), respectively. The four samples were then probe-sonicated (Ultrasonic Processor GEX500) for 120 min at 125 W. Subsequently they were centrifuged at 6000 rpm for 30 min at room temperature. The supernatants of four samples were collected and transferred into small glass vials for DLS measurements.

Characterizations and Measurements: Electrical characterizations were carried out using an ARS PSF-10-1-4 Cryogenic Probe Station and an Agilent E5270B analyzer at room temperature. Digital Instruments such as D3100 AFM, FEI Nova NanoSEM, and Hysitron TI950

Triboindenter SPM were used for investigating the film surface and cross-sectional morphologies. Raman spectra were obtained using a micro-Raman spectrometer (Renishaw InVia microscope) with a 1200 lines mm^{-1} blazed grating and a 1 mW laser excitation source at 514 nm. Acquisitions were carried out for 10 s with two averages using a 20× magnification lens. The nanoflake suspensions were diluted and their average lateral dimensions were measured using DLS technique (ALV 5022F spectrometer). The XRD patterns were collected using a Bruker D4 ENDEAVOR with monochromatic Cu Kα as radiation source ($\lambda = 0.154$ nm). The XPS was performed on a Thermo scientific K-Alpha instrument equipped with a monochromated aluminium K-α source (1486.7 eV). A pass energy of 20 eV was selected and the binding energy of the Mo2p peaks was shifted such that the adventitious C1s peak was aligned to 284.8 eV. The supernatant containing 2D molybdenum oxide flakes were dropped onto Cu grids for TEM and HRTEM (JEOL 2100F) characterization. The PESA measurements were conducted on drop-casted samples on glass slides and were measured using a Riken Keiki Model AC-2 PESA spectrometer with power setting of 100 nW and a power number of 1/3.

Supporting Information

Supporting Information is available from the Wiley Online Library or from the author.

Acknowledgements

The authors would like to acknowledge funding support from the Australian Research Council (ARC) through Discovery Project DP140100170. The authors also would like to acknowledge the facilities, scientific and technical assistances of the Australian Microscopy and Microanalysis Research Facility (AMMRF) at RMIT University, the Micro Nano Research Facility (MNRF) at RMIT University, and the Australian Centre for Materials Science and Engineering (CMSE) of the Commonwealth Scientific and Industrial Research Organization (CSIRO), Australia.

Received: September 1, 2015
Revised: September 29, 2015
Published online: November 20, 2015

[1] G. Fiori, F. Bonaccorso, G. Iannaccone, T. Palacios, D. Neumaier, A. Seabaugh, S. K. Banerjee, L. Colombo, *Nat. Nanotechnol.* **2014**, *9*, 768.
[2] D. Akinwande, N. Petrone, J. Hone, *Nat. Commun.* **2014**, *5*, 5678.
[3] Q. H. Wang, K. Kalantar-Zadeh, A. Kis, J. N. Coleman, M. S. Strano, *Nat. Nanotechnol.* **2012**, *7*, 699.
[4] S. Balendhran, S. Walia, H. Nili, J. Z. Ou, S. Zhuiykov, R. B. Kaner, S. Sriram, M. Bhaskaran, K. Kalantar-zadeh, *Adv. Funct. Mater.* **2013**, *23*, 3952.
[5] L. Li, Y. Yu, G. J. Ye, Q. Ge, X. Ou, H. Wu, D. Feng, X. H. Chen, Y. Zhang, *Nat. Nanotechnol.* **2014**, *9*, 372.
[6] X. Song, J. Hu, H. Zeng, *J. Mater. Chem. C* **2013**, *1*, 2952.
[7] B. Radisavljevic, A. Radenovic, J. Brivio, V. Giacometti, A. Kis, *Nat. Nanotechnol.* **2011**, *6*, 147.
[8] D. Lembke, A. Kis, *ACS Nano* **2012**, *6*, 10070.
[9] X. Liu, J. Hu, C. Yue, N. Della Fera, Y. Ling, Z. Mao, J. Wei, *ACS Nano* **2014**, *8*, 10396.
[10] B. Chamlagain, Q. Li, N. J. Ghimire, H.-J. Chuang, M. M. Perera, H. Tu, Y. Xu, M. Pan, D. Xaio, J. Yan, D. Mandrus, Z. Zhou, *ACS Nano* **2014**, *8*, 5079.
[11] J. Huang, L. Yang, D. Liu, J. Chen, Q. Fu, Y. Xiong, F. Lin, B. Xiang, *Nanoscale* **2015**, *7*, 4193.
[12] F. Schwierz, *Nat. Nanotechnol.* **2010**, *5*, 487.
[13] L. Yang, K. Majumdar, H. Liu, Y. Du, H. Wu, M. Hatzistergos, P. Y. Hung, R. Tieckelmann, W. Tsai, C. Hobbs, P. D. Ye, *Nano Lett.* **2014**, *14*, 6275.
[14] H. Fang, M. Tosun, G. Seol, T. C. Chang, K. Takei, J. Guo, A. Javey, *Nano Lett.* **2013**, *13*, 1991.
[15] H. Fang, S. Chuang, T. C. Chang, K. Takei, T. Takahashi, A. Javey, *Nano Lett.* **2012**, *12*, 3788.
[16] S. Balendhran, J. Deng, J. Z. Ou, S. Walia, J. Scott, J. Tang, K. L. Wang, M. R. Field, S. Russo, S. Zhuiykov, M. S. Strano, N. Medhekar, S. Sriram, M. Bhaskaran, K. Kalantar-zadeh, *Adv. Mater.* **2013**, *25*, 109.
[17] M. M. Y. A. Alsaif, S. Balendhran, M. R. Field, K. Latham, W. Wlodarski, J. Z. Ou, K. Kalantar-zadeh, *Sens. Actuators, B* **2014**, *192*, 196.
[18] M. Zhong, Z. Wei, X. Meng, F. Wu, J. Li, *Eur. J. Inorg. Chem.* **2014**, *2014*, 3245.
[19] M. M. Y. A. Alsaif, M. R. Field, B. J. Murdoch, T. Daeneke, K. Latham, A. F. Chrimes, A. S. Zoolfakar, S. P. Russo, J. Z. Ou, K. Kalantar-zadeh, *Nanoscale* **2014**, *6*, 12780.
[20] R. L. Smith, G. S. Rohrer, *J. Solid State Chem.* **1996**, *124*, 104.
[21] A. Pergament, V. Malinenko, L. Aleshina, E. Kazakova, N. Kuldin, *J. Exp. Phys.* **2014**, *2014*, 6.
[22] M. Doerr, J. Feller, H. Oppermann, *Cryst. Res. Technol.* **1996**, *31*, 231.
[23] E. B. Lopes, M. Almeida, J. Dumas, H. Guyot, C. Escribefilippini, *J. Phys.: Condens. Matter* **1992**, *4*, L357.
[24] E. Canadell, M. H. Whangbo, *Inorg. Chem.* **1990**, *29*, 2256.
[25] L. Kihlborg, *Acta Chem. Scand.* **1959**, *13*, 954.
[26] L. M. S. Alves, S. S. Benaion, C. M. Romanelli, C. A. M. dos Santos, M. S. da Luz, B. S. de Lima, F. S. Oliveira, A. J. S. Machado, E. B. Guedes, M. Abbate, R. J. O. Mossanek, *Braz. J. Phys.* **2015**, *45*, 234.
[27] F. Zeng, W.-B. Zhang, B.-Y. Tang, *Chin. Phys. B* **2015**, *24*, 097103.
[28] M. M. Y. A. Alsaif, K. Latham, M. R. Field, D. D. Yao, N. V. Medehkar, G. A. Beane, R. B. Kaner, S. P. Russo, J. Z. Ou, K. Kalantar-zadeh, *Adv. Mater.* **2014**, *26*, 3931.
[29] F. Torrisi, J. N. Coleman, *Nat. Nanotechnol.* **2014**, *9*, 738.
[30] S. Dasgupta, R. Kruk, N. Mechau, H. Hahn, *ACS Nano* **2011**, *5*, 9628.
[31] D. J. Finn, M. Lotya, G. Cunningham, R. J. Smith, D. McCloskey, J. F. Donegan, J. N. Coleman, *J. Mater. Chem. C* **2014**, *2*, 925.
[32] F. Torrisi, T. Hasan, W. Wu, Z. Sun, A. Lombardo, T. S. Kulmala, G.-W. Hsieh, S. Jung, F. Bonaccorso, P. J. Paul, D. Chu, A. C. Ferrari, *ACS Nano* **2012**, *6*, 2992.
[33] F. Withers, H. Yang, L. Britnell, A. P. Rooney, E. Lewis, A. Felten, C. R. Woods, V. S. Romaguera, T. Georgiou, A. Eckmann, Y. J. Kim, S. G. Yeates, S. J. Haigh, A. K. Geim, K. S. Novoselov, C. Casiraghi, *Nano Lett.* **2014**, *14*, 3987.
[34] J. Z. Ou, J. L. Carnpbell, D. Yao, W. Wlodarski, K. Kalantar-zadeh, *J. Phys. Chem. C* **2011**, *115*, 10757.
[35] R. Lampande, G. W. Kim, J. Boizot, Y. J. Kim, R. Pode, J. H. Kwon, *J. Mater. Chem. A* **2013**, *1*, 6895.
[36] S. N. Lou, N. Yap, J. Scott, R. Amal, Y. H. Ng, *Sci. Rep.* **2014**, *4*, 7428.
[37] M. E. Spahr, P. Novak, O. Haas, R. Nesper, *J. Power Sources* **1995**, *54*, 346.
[38] K. Kalantar-zadeh, J. Tang, M. Wang, K. L. Wang, A. Shailos, K. Galatsis, R. Kojima, V. Strong, A. Lech, W. Wlodarski, R. B. Kaner, *Nanoscale* **2010**, *2*, 429.

[39] Y. Wang, J. Z. Ou, A. F. Chrimes, B. J. Carey, T. Daeneke, M. M. Y. A. Alsaif, M. Mortazavi, S. Zhuiykov, N. Medhekar, M. Bhaskaran, J. R. Friend, M. S. Strano, K. Kalantar-Zadeh, *Nano Lett.* **2015**, *15*, 883.
[40] M. A. Camacho-Lopez, L. Escobar-Alarcon, M. Picquart, R. Arroyo, G. Cordoba, E. Haro-Poniatowski, *Opt. Mater.* **2011**, *33*, 480.
[41] G. Mestl, P. Ruiz, B. Delmon, H. Knozinger, *J. Phys. Chem.* **1994**, *98*, 11269.
[42] D. M. Koenhen, C. A. Smolders, *J. Appl. Polym. Sci.* **1975**, *19*, 1163.
[43] V. Nicolosi, M. Chhowalla, M. G. Kanatzidis, M. S. Strano, J. N. Coleman, *Science* **2013**, *340*, 6139.
[44] A. A. Ziabari, S. M. Rozati, *Physica B* **2012**, *407*, 4512.
[45] M. T. Greiner, L. Chai, M. G. Helander, W.-M. Tang, Z.-H. Lu, *Adv. Funct. Mater.* **2012**, *22*, 4557.
[46] C. Battaglia, X. Yin, M. Zheng, I. D. Sharp, T. Chen, S. McDonnell, A. Azcatl, C. Carraro, B. Ma, R. Maboudian, R. M. Wallace, A. Javey, *Nano Lett.* **2014**, *14*, 967.
[47] H. Wang, J. Luo, A. Robertson, Y. Ito, W. Yan, V. Lang, M. Zaka, F. Schaffel, M. H. Rummeli, G. A. D. Briggs, J. H. Warner, *ACS Nano* **2010**, *4*, 6659.
[48] S. Kim, A. Konar, W.-S. Hwang, J. H. Lee, J. Lee, J. Yang, C. Jung, H. Kim, J.-B. Yoo, J.-Y. Choi, Y. W. Jin, S. Y. Lee, D. Jena, W. Choi, K. Kim, *Nat. Commun.* **2012**, *3*, 1011.
[49] O. Katz, A. Horn, G. Bahir, J. Salzman, *IEEE Trans. Electron Devices* **2003**, *50*, 2002.
[50] K. Hirakawa, H. Sakaki, *Phys. Rev. B* **1986**, *33*, 8291.
[51] B. Macco, H. C. M. Knoops, W. M. M. Kessels, *ACS Appl. Mater. Interfaces* **2015**, *7*, 16723.
[52] N. Preissler, O. Bierwagen, A. T. Ramu, J. S. Speck, *Phys. Rev. B* **2013**, *88*, 085305.
[53] N. Ma, D. Jena, *Phys. Rev. X* **2014**, *4*, 011043.
[54] W. Zhu, T. Low, Y.-H. Lee, H. Wang, D. B. Farmer, J. Kong, F. Xia, P. Avouris, *Nat. Commun.* **2014**, *5*, 3087.
[55] B. Dasgupta, Y. Ren, L. M. Wong, L. Kong, E. S. Tok, W. K. Chim, S. Y. Chiam, *J. Phys. Chem. C* **2015**, *119*, 10592.